

裂纹位置对强度失配焊接接头极限载荷的影响

段小雪¹, 张彦华¹, 熊林玉², 田志杰², 苏志强²

(1. 北京航空航天大学 机械工程及自动化学院, 北京 100191; 2. 首都航天机械公司, 北京 100076)

摘要: 采用有限元方法对平面应变条件下含裂纹的强度失配焊接接头极限载荷进行了计算, 研究了裂纹位于焊缝不同位置时对接头极限载荷的影响. 结果表明, 裂纹尺寸和焊缝宽度增大时, 接头极限载荷接近均质焊缝的极限载荷, 此时失配系数的影响很大; 裂纹尺寸和焊缝宽度减小, 不同失配系数接头的极限载荷逐渐趋于一致. 当焊缝强度失配程度一定时, 裂纹偏置量在裂纹尺寸较大且焊缝较宽时对接头极限载荷的影响较大, 裂纹偏置量增大可使低匹配接头极限载荷提高, 对高匹配接头则相反. 随着裂纹尺寸和焊缝宽度的减小, 裂纹偏置量对接头极限载荷的影响程度减弱.

关键词: 强度失配; 裂纹偏置; 极限分析; 极限载荷; 有限元法

中图分类号: TG407 **文献标识码:** A **文章编号:** 0253-360X(2013)06-0093-04



段小雪

0 序 言

焊接接头焊缝与母材的力学性能差异所导致的强度失配对含裂纹焊接结构的断裂参量^[1]及极限载荷等有显著的影响. 在焊接接头的缺陷评定中, 结构的极限载荷^[2,3]是关系评定结果准确与否至关重要的参量, 因而准确确定强度失配焊接接头的极限载荷是非常重要的. Hao 等人^[4,5]采用滑移线场 (slip line field, SLF) 理论对不同失配系数及几何条件的焊缝中心裂纹平板拉伸试件进行了平面应变有限元极限载荷分析, 得到了失配极限载荷解. 然而由于多种塑性变形方式的存在且涉及到的参量很多, 基于 SLF 的分析一时也不可能给出全面的结果. Kim 等人^[6-8]用有限元法, 得到了弹性理想塑性材料裂纹位于焊缝中心、母材和焊缝界面时, 不同形式的焊接接头的极限载荷, 认为尽管有限元法费时却能给出精确的结果. 到目前为止, 大多数的研究结果是基于对称裂纹(裂纹位于焊缝中心)的, 而在实际中, 裂纹可能位于焊缝中的不同位置, 因此研究裂纹位置对强度失配焊接接头的断裂行为是非常必要的.

焊接接头的极限载荷求解涉及到强度失配、裂纹长度、焊缝宽度等参量, 很难得到完全解, 通常采用上限定理分析, 这需要具备深入的理论知识和技巧. Lei 等人^[9]和 Andrei 等人^[10]用下限法对含非对

称裂纹接头的极限载荷进行了理论分析. 随着计算机功能的强大, 以增量有限元方法为代表的数值计算方法显示出强大的威力, 与理论分析相比, 有限元能够得到更精确的解. 文中采用有限元方法对平面应变条件下裂纹位置变化的焊接接头极限载荷进行了计算分析.

1 含非对称裂纹焊接接头有限元模型

焊接接头由母材、焊缝、热影响区组成, 各区组织结构及性能不同, 且存在残余应力, 将所有现实因素考虑完全来对焊接接头进行分析几乎是不可能的, 因此对模型进行简化. 根据焊接结构完整性分析的实际需要, 文中选用平板对接接头, 简化为双材料模型, 忽略热影响区. 焊接残余应力是焊接接头固有的特点, 其大小和分布与具体焊接方法、参数、焊后热处理方式等有很大关系, 而且当存在裂纹时会使残余应力重新分布或释放, 在塑性变形较大时影响不大, 因此文中不考虑残余应力的影响. 模型尺寸为长度 $2L = 160 \text{ mm}$ 、宽度 $2W = 80 \text{ mm}$, 焊缝宽度为 $2H$, 裂纹长度为 $2a$. 裂纹位于焊缝中, 关于试件宽度方向对称, 距离试件长度方向焊缝中心的距离为 h , 定义 h 与焊缝半宽 H 的比为偏置系数 e , $e = 0$ 代表裂纹位于焊缝中心, $e = 1$ 代表裂纹位于焊缝与母材界面, 文中 $0 < e < 1$.

通常将焊缝屈服强度 (R_{eLW}) 与母材屈服强度 (R_{eLB}) 的比定义为强度失配系数, 用 M 来表示, $M >$

1 为高匹配, $M < 1$ 为低匹配. 对于均质材料, 塑性变形模式取决于裂纹尺寸和加载形式. 对于失配焊接接头来说, 塑性变形模式则要复杂的多, 焊缝和母材的失配系数 M 以及韧带与焊缝半宽 H 之比 $\psi = (W - a) / H$ 也是重要的影响因素.

材料设定为各向同性理想弹塑性模型, 设焊缝和母材的弹性模量均为 210 GPa, 泊松比为 0.3, 母材屈服强度 $R_{eLB} = 500$ MPa, 改变焊缝屈服强度, 使 $M = 0.5, 0.6, 0.8, 1.2, 1.4, 2.0$. 偏置系数 $e = 0.25, 0.5, 0.75$. 裂纹长度 $2a$ 取 2, 8, 16, 24, 32, 40, 64 mm. 焊缝宽度 $2H$ 取 4, 8, 16, 24, 32, 36 mm.

采用 ABAQUS 软件进行平面应变条件下弹塑性有限元分析. 由于实际裂纹尖端不可能是无限尖的, 所以使用了裂尖半径为 0.005 mm 的钝化裂纹模型. 利用模型对称性, 对 1/2 模型进行分析, $a/W = 0.3$, $2H = 24$ mm, $e = 0.5$ 的有限元网格如图 1 所示, 共 6 059 个节点、1 948 个单元, 单元类型为 8 节点平面应变缩减积分单元 CPE8R. 施加足够大的位移载荷, 使其达到极限状态, 根据载荷与加载点位移曲线得到极限载荷值. 在计算时考虑几何非线性的影响, 在达到极限状态后, 位移继续增大而载荷开始下降, 选择载荷—加载点位移曲线中的最大值作为极限载荷.

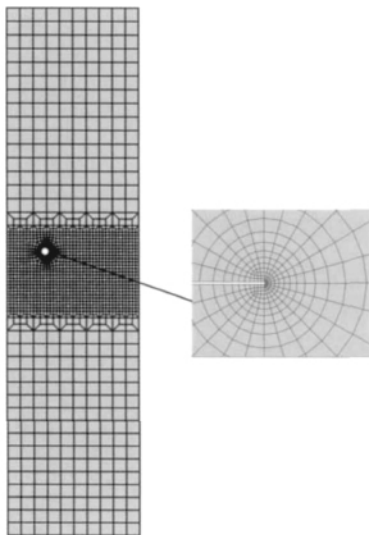


图 1 有限元网格及裂纹尖端放大图

Fig. 1 Finite element mesh and crack tip

2 计算结果分析

2.1 屈服模式

分别对不同 M 、 ψ 及 e 值组合的模型进行了大

量的有限元计算. 结果表明, 不同裂纹位置时强度失配焊接接头的塑性屈服模式有以下几种.

(1) 低匹配: ①塑性变形带变形完全被限制在焊缝中(图 2a); ②塑性变形带一侧在焊缝中一侧穿过母材(图 2b); ③塑性变形带的两侧都穿过母材(图 2c).

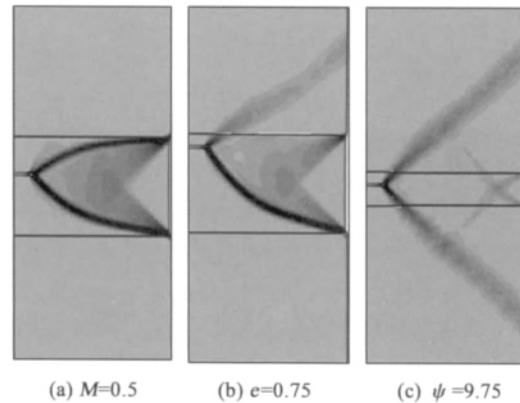


图 2 低匹配接头的屈服模式

Fig. 2 Plastic deformations patterns of under-matched joints

当焊缝与母材的强度失配系数 M 很低时, 塑性变形往往被限制在焊缝中; 当 M 很低而偏置系数 e 较大就会出现塑性变形带一侧在焊缝中一侧穿过母材的情况; 如果焊缝较窄, 则塑性变形带两侧均会穿过母材.

(2) 高匹配: ①塑性变形带变形完全被限制在焊缝中(图 3a); ②塑性变形带一侧在焊缝中一侧穿过母材(图 3b); ③塑性变形带两侧变形都穿过母材(图 3c); ④全面屈服(图 3d).

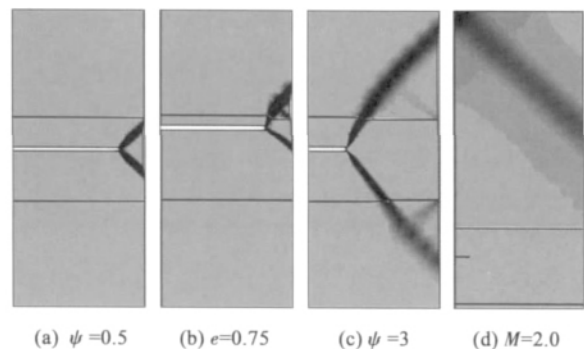


图 3 高匹配接头的屈服模式

Fig. 3 Plastic deformation patterns of over-matched joints

当 ψ 很小且裂纹靠近焊缝中心的情况下, 塑性变形往往被限制在焊缝中; 如果裂纹很长、焊缝较宽且偏置系数较大, 即 ψ 很小 e 较大时就会出现塑性

变形带一侧在焊缝中一侧穿过母材的情况; 如果裂纹长度适中, 则塑性变形带两侧变形均会穿过母材; 当焊缝与母材的强度失配系数 M 较高且裂纹尺寸较小时, 会发生全面屈服。

2.2 极限载荷分析

图 4 和图 5 分别为偏置系数一定和失配系数一定的情况下, 不同接头的 ψ 与 F_{YM}/F_{YB} 关系曲线, 其中 F_{YM} 为失配接头的极限载荷, F_{YB} 为同样几何尺寸下均质母材的极限载荷。从图 4 中可以看出, 当 ψ 较小即裂纹较短且焊缝较宽时, 接头极限载荷接近均质焊缝的极限载荷, 此时失配系数的影响很大; 从图 4 中可以看出, 当 ψ 较小即裂纹较短且焊缝较宽时, 接头极限载荷接近均质焊缝的极限载荷, 此时失配系数的影响很大, 这是由于变形被限制在焊缝中, 接头的极限载荷取决于焊缝的承载能力; 随着 ψ 的增大, 裂纹尖端区塑性变形跨越焊缝进入母材, 强度失配系数的影响逐渐减小; ψ 继续增大, 强度失配系数的影响进一步降低, 不同强度失配系数接头的极限载荷趋于一致, 也就是说裂纹尺寸越小且焊缝越窄, 失配系数的影响越小。当失配系数 M 一定时, 偏置系数在 ψ 较小时对接头极限载荷的影响较大, 对于低匹配来说偏置系数增大极限载荷提高, 高匹配则正好相反, 此后随着 ψ 的增大, 不同偏置系数接头的极限载荷趋于一致。

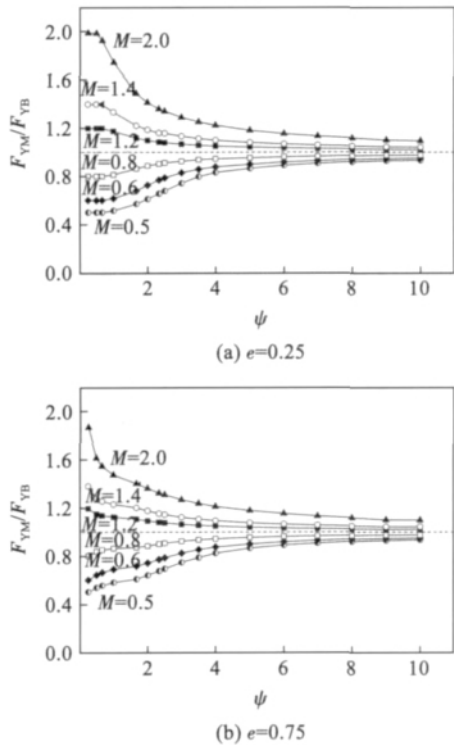


图 4 偏置系数一定时不同失配系数接头的极限载荷
Fig. 4 Limit loads of mis-matched welded joints for a given crack eccentricity

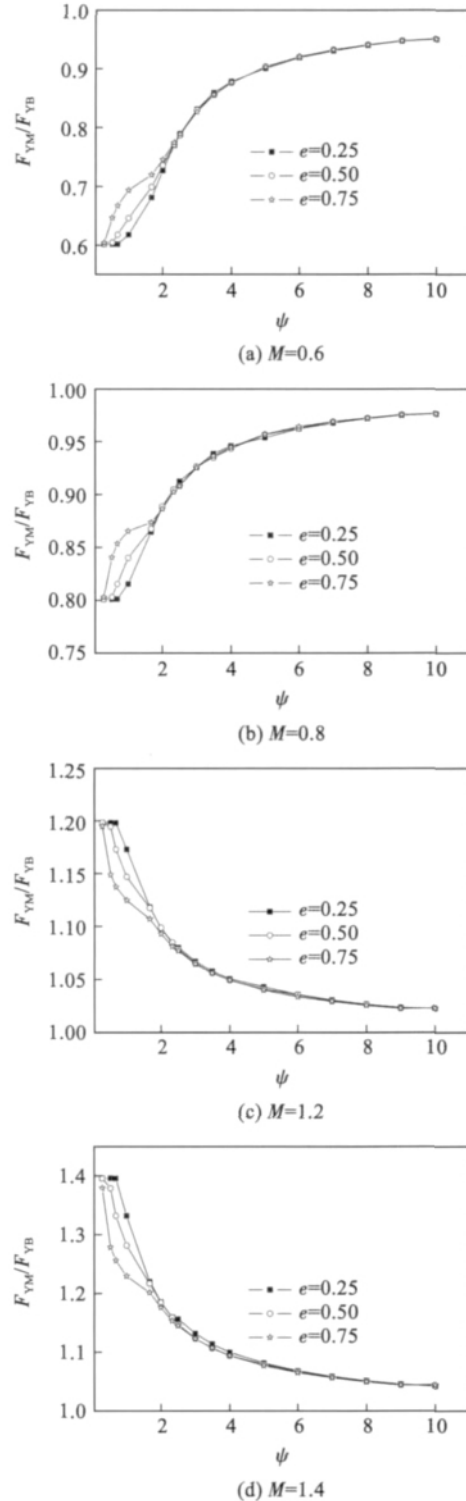


图 5 失配系数一定时不同偏置系数接头的极限载荷
Fig. 5 Limit loads of welded joints with different crack eccentricity for a given strength mis-match factor

3 结 论

(1) 低匹配焊接接头的塑性屈服模式有 3 种情形, 当 M 很低时, 变形往往被限制在焊缝中; 当 M 较低且偏置系数 e 较大就会出现变形一侧在焊缝中一

侧穿过母材的情况;如果焊缝较窄,则两侧变形均会穿过母材。

(2) 高匹配焊接接头的塑性屈服模式有4种情形,当 M 较高且裂纹尺寸较小时,会发生全面屈服;如果裂纹较长、焊缝较宽且偏置系数 e 较大,就会出现变形一侧在焊缝中一侧穿过母材的情况;如果裂纹长度适中,则两侧变形均会穿过母材;在 ψ 很小且 e 较大的情况下,变形也会被限制在焊缝中。

(3) 当 ψ 很小即裂纹很长且焊缝较宽时,接头极限载荷接近均质焊缝的极限载荷,此时失配系数的影响很大;随着 ψ 的增大,不同失配系数接头的极限载荷逐渐趋于一致,也就是说裂纹尺寸越小且焊缝越窄,失配系数的影响越小。

(4) 当 M 一定时,偏置系数在 ψ 较小时对接头极限载荷的影响较大,对于低匹配来说偏置系数增大极限载荷提高,高匹配则正好相反,此后随着 ψ 的增大,不同偏置系数接头的极限载荷趋于一致。

参考文献:

- [1] 熊林玉,张彦华. 强度失配焊接接头的裂纹尖端张开位移数值分析[J]. 焊接学报, 2012, 33(4): 93-96.
Xiong Linyu, Zhang Yanhua. Numerical analysis on crack tip opening displacement of strength mismatched welded joint [J]. Transactions of the China Welding Institution, 2012, 33(4): 93-96.
- [2] 刘明亮,张玉凤,霍立兴,等. 海底管道高匹配焊接接头的安全评定[J]. 焊接学报, 2006, 27(5): 31-34.
Liu Mingliang, Zhang Yufeng, Huo Lixing, et al. Safe assessment for overmatching welded joint of offshore pipeline [J]. Transactions of the China Welding Institution, 2006, 27(5): 31-34.
- [3] 刘明亮,张玉凤,霍立兴,等. 海底管道安全性评定方法的分析[J]. 焊接学报, 2006, 27(8): 75-78.
Liu Mingliang, Zhang Yufeng, Huo Lixing, et al. Methods of safe assessment for offshore pipeline [J]. Transactions of the China Welding Institution, 2006, 27(8): 75-78.
- [4] Hao S, Cornec A, Schwalbe K H. Plastic stress-strain fields and limit loads of a plane strain cracked tensile panel with a mismatched welded joint [J]. International Journal of Solids and Structures, 1997, 34(3): 297-311.
- [5] Hao S, Schwalbe K H, Cornec A. The effect of yield strength mis-match on the fracture analysis of welded joints: slip-line field solutions for pure bending [J]. International Journal of Solids and Structures, 2000, 37(39): 5385-5411.
- [6] Kim Y J, Schwalbe K H. Mismatch effect on plastic yield loads in idealised weldments I. Weld center cracks [J]. Engineering Fracture Mechanics, 2001, 68(2): 163-182.
- [7] Kim Y J, Schwalbe K H. Mismatch effect on plastic yield loads in idealised weldments II. Heat affected zone cracks [J]. Engineering Fracture Mechanics, 2001, 68(2): 183-199.
- [8] Kim Y J, Schwalbe K H. Compendium of yield load solutions for strength mis-matched DE(T), SE(B) and C(T) specimens [J]. Engineering Fracture Mechanics, 2001, 68(9): 1137-1151.
- [9] Lei Y, Tao J, Li P N. Limit load and J estimates of a center cracked plate with an asymmetric crack in a mismatched weld [J]. International Journal of Pressure Vessels and Piping, 1999, 76(11): 747-757.
- [10] Andrei K, Mohd F, Mohamed J. Collapse load for a crack in a plate with a mismatched welded joint [J]. Engineering Failure Analysis, 2006, 13(7): 1065-1075.

作者简介: 段小雪,女,1978年出生,博士研究生.主要从事焊接结构疲劳与断裂方面的研究.发表论文3篇. Email: snowf220@126.com

通讯作者: 张彦华,男,教授. Email: zhangyh@buaa.edu.cn

pp 73 – 76

Abstract: 7075-T6 aluminum alloy was successfully spot joined by refill friction stir spot welding process. The microstructure, microhardness, tensile/shear strength and cross-tension strength of the joints were tested. Experimental results indicate that the microstructure can be divided into the nugget zone, thermo-mechanically affected zone, heat-affected zone and base material, respectively. Defects such as hook, cavity, incomplete fusion, incomplete refill and bonding ligament were found in the joint. The microhardness profile in the welded zone exhibited W-shaped appearance, but that in the stir zone exhibited V-shaped appearance. When the rotational speed was 1 400 r/min, the highest tensile/shear strength reached 7 916.0 N, which was 39.6% of the base material. The change of the cross-tension strength with the processing parameters was complicated, and the highest cross-tension strength can reach 43.9 MPa.

Key words: aluminum alloy; friction spot welding; microstructure; mechanical property

Effect of precoating on microstructure of SiC reinforced iron-based coating

GAO Zhen, DU Xiaodong, WANG Jinjia, SONG Zili (School of Materials Science and Engineering, Hefei University of Technology, Hefei 230009, China). pp 77 – 80

Abstract: The reaction layers consisting of Cr_3Si , Cr_7C_3 and Cr_{23}C_6 were produced on SiC surface by PIRAC technology. The iron-based alloy coating reinforced by precoated SiC particles was prepared by plasma surfacing process with the back-feeding model. The results show that the non-precoated SiC particles dissolve completely in the coating. Massive primary polygonal carbides formed in the upper part, dendrites formed in the middle part and cellular grains generated in the bottom part. The precoated SiC particles distributed in the coating surface, retaining the original shape, and did not dissolve significantly. The region between SiC particles and the matrix could be divided into the interface reaction zone and the transition zone. The interface reaction zone consisted of α -(Fe, Cr) solid solution, massive (Fe, Cr) $_7\text{C}_3$ and (Fe, Cr) $_{23}\text{C}_6$ carbides. The transition zone consisted of the α -(Fe, Cr) solid solution with high Cr content, and it was difficult to expose the microstructure due to its excellent corrosion resistance.

Key words: SiC; precoating; microstructure; interface reaction

Analysis of orthogonal test of properties of dual-phase DP600 steel resistance spot welded joint

TAO Bohao¹, LI Hong¹, SONG Yonglun², LI Qiang² (1. School of Materials Science and Engineering, Beijing University of Technology, Beijing 100124, China; 2. School of Mechanical Engineering and Applied Electronics Technology, Beijing University of Technology, Beijing 100124, China). pp 81 – 84

Abstract: The spot welding parameters for cold-rolled dual-phase DP600 steel in industrial trial production were optimized by orthogonal experimental design method with the tensile/shear loads of spot welded joints as the evaluation index. The welding window and optimal welding parameters were achieved by range analysis and variance analysis. The microstructure and tensile/shear loads of the spot welded joints under optimized welding parameters were investigated. The results showed that the welding current was between 9 000 A and 12 000 A, and the welding time was between 200 ms and 500 ms in the welding window.

The welding current had most remarkable influence on the joint strength. With the increase of welding current, the tensile/shear loads increased. The maximum load 14 kN and the maximum absorbing energy 45.26 kJ were obtained with 12 000 A welding current, 200 ms welding time and 2 500 N electrode pressure. And the microstructure of the resultant welded nugget mainly consisted of lath martensite.

Key words: resistance spot welding; DP600 steel; orthogonal experiment design; range analysis; variance analysis

Release coefficients during measuring non-uniform residual stress with blind-hole method

LI Hao, LI Hua (School of Civil and Hydraulic Engineering, Hefei University of Technology, Hefei 230009, China). pp 85 – 88

Abstract: Integral method is widely used in calculating the non-uniform residual stresses from the measured relaxed strains using the blind-hole method, in which the release coefficients have great influence on the measurement accuracy. As the residual stresses in each layer are assumed to be uniform when calibrating the coefficients, the calculated results are considerably different from the real stresses if the residual stresses vary rapidly along the depth. In this paper, a three-dimensional FEM model was established for the release coefficients, and verified by a simulated test on a uniform loaded plate. The errors in the calculation of the non-uniform residual stress field were studied using the release coefficients calibrated by the integral method, and then an improved technique was proposed to recalibrate the release coefficients. The results show that the calculated residual stresses using the recalibrated coefficients are closer to the real ones.

Key words: blind-hole method; non-uniform residual stress; integral method; release coefficient; recalibration

Finite element simulation of rectifying roundness of welded thin-walled cylinder by extrusion

LI Jun^{1,2}, ZHANG Wenfeng¹, FANG Hongyuan² (1. Zhejiang Yinlun Machinery Company Ltd., Tiantai 317200, China; 2. State Key Laboratory of Advanced Welding and Joining, Harbin Institute of Technology, Harbin 150001, China). pp 89 – 92

Abstract: The method of rectifying the roundness of welded thin-walled cylinders was proposed by extruding the metal in and around the weld. The effect of roundness rectification by extrusion and the mechanism in which the effect lies were investigated by finite element method (FEM). The cylinder welded longitudinally has a peach shape in radial direction and significantly distorts at two ends. The simulation results show that the extrusion method can effectively improve the roundness of the welded cylinder. The effectiveness of rectifying the roundness of welded thin-walled cylinders by extrusion was verified with self-made devices. The experimental results show that the roundness at the ends of welded stainless steel cylinders with 2 mm in wall thickness, 300 mm in length and 280 mm in external diameter can be reduced to about 0.5 mm by extruding the metal in and around the weld.

Key words: welding; thin wall; cylinder; extrusion; numerical simulation

Effect of crack location on limit loads of strength mismatched welded joints

DUAN Xiaoxue¹, ZHANG Yanhua¹, XIONG Linyu², TIAN Zhijie², SU Zhiqiang² (1. School of Mechanical Engineering and Automation, Beihang University, Beijing 100191,

China; 2. Capital Aerospace Machinery Company , Beijing 100076 , China) . pp 93 – 96

Abstract: Limit loads of strength mismatched welded joints with asymmetric cracks were calculated using finite element method , and the effect of crack location on the limit load of strength mismatched welded joint was investigated. The results show that when the weld slenderness (the ratio of crack ligament to the half-weld width) was small , the limit load of welded joint was close to that of homogeneous welded metal plate with the same geometry. With the increase of slenderness , the limit load of welded joints with different strength mismatched factors converged and the influence of strength mismatching decreased. For a given strength mismatched factor , crack eccentricity had great influence on the limit load of welded joint when the weld slenderness was small , the limit load of under-matched joint increased with the increase of crack eccentricity , while for over-matched joint , the opposite was true. With the increase of weld slenderness , the effect of crack eccentricity on the limit load decreased.

Key words: strength mismatch; asymmetric crack; limit analysis; limit load; finite element method

Influence of Mn on microstructure and properties of vertically welded joint with pulse combustion welding rod

WU Yongsheng¹ , WANG Jianjiang¹ , XIN Wentong¹ , QU Lifeng² (1. The Institute of Advanced Materials , Ordnance Engineering College , Shijiazhuang 050003 , China; 2. Military Delegate Office of Chongqing Martial Delegate Agency in No. 167 Factory , Chengdu 610110 , China) . pp 97 – 100

Abstract: Q235 steel was welded by manual high-temperature synthesis (SHS) vertical welding process with pulse combustion welding rod , and the influence of Mn content on the microstructure and properties of the resultant joints were studied. The results show that , without adding Mn in the pulse combustion welding rod , massive pores appeared in the weld without forming effective weld pool at the starting position of welding. When the Mn content was less than 5.9 wt% , the higher the Mn content was , the better the weld was shaped , and the pores reduced rapidly. Fe-rich phases dominated in the weld with the proportion increasing with the increase of Mn content , and the mechanical properties of the joints also increased. When the Mn content was 5.9wt% , the mechanical properties of the joints reached the optimum with tensile strength of 421 MPa and microhardness of 1 578.8 MPa. When the Mn content exceeded 5.9wt% , the increase of Mn content resulted in the weld pool flowing downward seriously and forming welding beading or even burning through the substrate. The resulting weld mainly comprised Cu-rich phases with lots of cracks , which deteriorated the mechanical properties of the joint.

Key words: plus combustion welding rod; vertical welding; microstructure

Narrow gap pulsed MAG welding of 40CrMnMo thick-walled pipe

BA Lujun¹ , MA Caixia² , ZHANG Tiejun¹ , WANG Jun¹ , WANG Qinglin¹ (1. Drilling Pipe and Tools Company , Shengli Petroleum Administration Bureau Bohai General Drilling Company , Dongying 257200 , China; 2. Shaanxi Key Laboratory of Friction Welding Technologies , Northwestern Polytechnical University , Xi'an 710072 , China) . pp 101 – 104

Abstract: Considering the structure characteristics of small-diameter thick-walled pipe and the properties of 40CrMnMo steel , narrow gap pulsed MAG welding technique was preferred

to weld the oil drill collars. A large number of experiments were conducted to improve the gas protection , arc morphology and stability , and weld appearance to avoid the sidewall fusion defects during welding , and the narrow gap multi-layer welding parameters were optimized. Furthermore , a new special narrow gap welding torch was designed , which had advantages such as simple and compact structure , good accessibility , good gas protection , easy ignition , stable arc combustion and free from sidewall ignition. The mechanical tests and microstructure analysis show that the mechanical properties of joints can satisfy the practical requirements of the oil drill collars.

Key words: oil drill collars; narrow gap pulsed MAG welding; weld appearance; joint property

Numerical simulation of resistance spot welding of three-layer galvanized steel sheets

LU Changjin¹ , TANG Hong¹ , YAO Qiwei² , YU Miao² , SHEN Qing² , LEI Ming³ (1. Shanghai Key Laboratory of Laser Manufacturing & Material Modification , Shanghai Jiaotong University , Shanghai 200240 , China; 2. SGM Dongyue , Dongyue 264006 , China; 3. Baoshan Iron and Steel Co. , Ltd. , Shanghai 201900 , China) . pp 105 – 108

Abstract: Based on the characteristics of resistance spot welding of three-layer sheets and properties of zinc coating , 1/4 model was established to numerically simulate the three-layer sheets. On the basis of experimental parameters , the nugget was investigated through optimizing the parameters. Then under the peak temperature , nugget formation and growth in different materials were analyzed with the optimized parameters. It was found that , comparing to the sheets without Zn coating , the Zn coating can affect the nugget formation , change the location of nugget nucleation and growing trend. For three-layer galvanized sheets , the nugget initially formed in the interface between two sheets without Zn coatings , and then grew radially and axially , finally penetrated three sheets. The simulated results agreed well with the experimental results.

Key words: spot welding; three layer board; numerical simulation; zinc coating; nugget

Analysis of buckling distortion caused by welding using 3D optical measurement technology

SUN Xiangwei¹ , YIN Xianqing¹ , WANG Jiangchao² , ZHANG Jianxun¹ (1. State Key Laboratory for Mechanical Behavior of Materials , Xi'an Jiaotong University , Xi'an 710049 , China; 2. Joining and Welding Research Institute , Osaka University , Osaka 5670047 , Japan) . pp 109 – 112

Abstract: 3D optical surface scanning method was used in this paper to investigate the buckling distortion of mild-steel plate during bead-on welding. The full field distortions were obtained through measuring the deformation of the plate before and after welding , respectively. Based on the numerical simulation on the elastic buckling distortion with inherent strain method , it was found that the concave-convex type distortion belonged to buckling distortion. The residual stresses were measured with hole-drilling method , and the results showed that the high longitudinal compressive stress existed in the zone away from the weld , which resulted in the buckling distortion of the plate. Combining with numerical simulation , the 3D optical surface scanning system could be used to accurately investigate the buckling mechanism of welded thin plate.

Key words: 3D optical surface scanning; thin plate; GTAW; buckling distortion; inherent strain method